



Research Article

The effect of a New Hybrid Severe Plastic Deformation Method on the Microstructure and Mechanical Properties of CP-Ti

Behzad Pasoodeh¹, Vali Alimirzaloo^{*1} , Mehrdad Shahbaz² , Kaveh Hajizadeh³ and Javad Alizadeh Kaklar¹

¹ Department of Mechanical Engineering, Faculty of Engineering, Urmia University, Urmia, Iran

² Department of Materials Science and Engineering, Faculty of Engineering, Urmia University, Urmia, Iran

³ Faculty of Mining and Metallurgical Engineering, Urmia University of Technology, Urmia, Iran

ARTICLE INFO

Article history:

Received: 29 April 2025

Reviewed: 29 June 2025

Revised: 16 September 2025

Accepted: 21 September 2025

Keywords:

New CECAP

Mechanical properties

CP-Ti

Finite element analysis

Please cite this article as:

Pasoodeh, B., Alimirzaloo, V., Shahbaz, M., Hajizadeh, K., & Alizadeh Kaklar, J. (2025). The effect of a new hybrid severe plastic deformation method on the microstructure and mechanical properties of CP-Ti. *Iranian Journal of Materials Forming*, 12(4), 54-65. <https://doi.org/10.22099/ijmf.2025.53087.1331>

ABSTRACT

In the present study, a novel combined process of severe plastic deformation (SPD) process was introduced, and its effects on the flow behavior, workability, and mechanical properties of commercially pure titanium were investigated through a single-pass billet deformation. The process consists of three sequential stages: primary cyclic extrusion compression (CEC), equal channel angular pressing (ECAP), and final extrusion. The results showed that the average hardness of the annealed, as-received specimens was 14 HRC on the section perpendicular to the movement axis. This value increased to 21 HRC, 26 HRC, and 29.5 HRC in samples processed by ECAP, CECAP, and the New CECAP process, respectively. These results demonstrate the superior effectiveness of the New CECAP process in enhancing hardness. Moreover, the findings revealed that the New CECAP process improves the strain distribution compared to CECAP and ECAP, with maximum strain increasing by up to 15% and 23%, respectively.

© Shiraz University, Shiraz, Iran, 2025

1. Introduction

To obtain ultrafine-grained and bulk nanostructured materials, severe plastic deformation (SPD) methods have been significantly developed. Numerous approaches have been proposed to achieve ultrafine microstructures. As a result, improving these methods

has attracted considerable attention from researchers [1–3]. Titanium and its alloys, such as Ti–6Al–4V, possess excellent properties, including corrosion resistance, mechanical strength, and biocompatibility, making them widely used in the fabrication of biomedical devices. Consequently, these materials have received significant

* Corresponding author

E-mail address: v.alimirzaloo@urmia.ac.ir (V. Alimirzaloo)

<https://doi.org/10.22099/ijmf.2025.53087.1331>

attention in research. Titanium alloys (e.g., Ti-6Al-4V) offer superior properties compared to commercially pure titanium (CP-Ti). However, the alloying elements in Ti-6Al-4V can release toxic metal ions, resulting in limited biocompatibility for medical applications [4]. Therefore, CP-Ti is considered a suitable alternative for biomedical use, provided that its strength is enhanced, something that can be achieved through SPD methods. One such method is CECAP (cyclic extrusion compression angular pressing), which is capable of producing ultrafine microstructures [5–8]. This technique can reduce the grain size of CP-Ti to below 1 μm , thereby improving strength and achieving an ultrafine-grained titanium (UFGTi) structure suitable for medical applications [9–10]. Equal channel angular pressing (ECAP) is one of the most well-known SPD methods, extensively used to produce ultrafine microstructures. It has been applied to a wide variety of metallic materials, including Al-Mg alloys, Pb-Sn alloys, AZ91, AZ31, and titanium alloys [11–13]. Despite its advantages, ECAP suffers from strain inhomogeneity across the processed samples, which is regarded as one of its major drawbacks [14]. Cyclic extrusion compression (CEC) is another SPD technique capable of introducing greater plastic deformation. In this method, each pass involves both extrusion and compression. However, the application of back pressure is required to restore the deformed sample to its original shape, and this is regarded as a key limitation of the method [15–17].

To overcome the individual drawbacks of ECAP and CEC, the CECAP method was introduced, combining the advantages of both. In CECAP, the compression-extrusion operation is first applied to a cylindrical sample (e.g., 15 mm in diameter). The deformed sample then enters the ECAP region. Due to the pressure applied by ECAP, the sample is forced to fill the space between the ECAP and CEC sections, effectively restoring its original shape (diameter of 15 mm). This method was first developed by M. Ensafi et al. [8], who studied its effects on the AZ91 alloy. Their results showed that grain refinement occurred mainly near the outer layers, and the total strain was equal to the sum of the strains from both CEC and ECAP. While this

method introduced greater plastic deformation, it suffered from relatively low hydrostatic compression stress, identified as a disadvantage. To address this, Ahmadi et al. [9] proposed a New CECAP method, aimed at improving both the hydrostatic compression stress and strain uniformity. In this approach, an additional extrusion zone was added to the horizontal channel, which compensated for the shortcomings in hydrostatic pressure and strain distribution. The effectiveness of this method was demonstrated using an Mg alloy, with grain refinement and stress metrics as response variables. The New CECAP process resulted in a 50% increase in average compressive stress compared to the conventional CECAP. Furthermore, the mechanical properties and microstructure of AM60 magnesium alloy were analyzed using the New CECAP method [19]. After four passes, hardness increased by 196% for the New CECAP and by 175% for the conventional CECAP, compared to the unprocessed samples. A model was also proposed to integrate strength and damping performance, considered a key challenge for broader use of Mg alloys/composites, by evaluating the effect of the CEC method and the addition of carbon nanotubes (CNTs) on the damping behavior of AZ91D alloy [20]. The results showed that, below a critical temperature, damping was primarily enhanced by dislocation movement between sparse strong pinning points and numerous weak ones. Ebrahimi et al. [21] explored damping performance in SiC nanoparticle-reinforced AZ91D composites (SiCnp/AZ91D) processed via CEC. They found that the CEC process significantly influenced damping behavior due to changes in dislocation density and grain boundary distribution in the matrix alloy. In a related study, Huang et al. [22] investigated how torsion-bending ratio, axial compression, and eccentricity affect the mechanical behavior of reinforced concrete (RC) columns under combined loadings. Finite element modeling (FEM) results revealed decreased seismic performance as eccentricity increased from 0.125 to 0.25. The results also highlighted the significant negative impact of torque on the mechanical behavior.

The mechanical properties of ECAP-processed

samples have garnered widespread attention. However, inhomogeneity in ECAP-processed samples remains a concern. To address this issue, the CECAP method was developed. Accordingly, this study presents a comparative analysis of ECAP, CECAP, and New CECAP processes in terms of mechanical and microstructural characteristics. Notably, previous studies have not applied the CECAP method to CP-Ti; therefore, this research investigates the effects of these methods on CP-Ti for the first time. Additionally, the Finite element method (FEM) was used to simulate the process via DEFORM-3D, and the simulation results were compared with experimental data.

2. New CECAP Process Principle

A schematic representation of the New CECAP process is illustrated in Fig. 1. This setup consists of two interchangeable extrusion inserts located before and after the ECAP deformation zone. The die is composed of two cylindrical channels with a diameter of 15 mm and an ECAP deformation region characterized by a channel angle of 90° and a corner angle of 20° (Here, D denotes the initial specimen diameter, E the input CEC diameter, and X the exit extrusion diameter). At the beginning of the process, the input CEC zone applies a 2 mm diameter reduction to the initial 15 mm sample. Due to the resistance at the end of the vertical cylindrical ECAP channel, the sample tends to expand and restore its original geometry (15 mm diameter). In the next stage, the sample passes through the ECAP region, where it undergoes further plastic deformation. Finally, the

sample enters the exit extrusion zone at the end of the horizontal channel. In this region, an additional 1 mm diameter reduction is applied, which also generates extra back pressure during the New CECAP process. These three stages, input CEC, ECAP, and exit extrusion, are sequentially applied to the sample. Therefore, the total strain imposed on the sample in the New CECAP process is the cumulative result of the three operations, expressed by Eqs. (1), (2), and (3) [8, 9]. Consequently, Eq. (4) is derived to represent the total strain applied during one pass of the New CECAP process:

$$\varepsilon_{ECAP} = 1/\sqrt{3} \{2 \cot(\varphi/2 + \psi/2) + \psi \csc(\varphi/2 + \psi/2)\} \quad (1)$$

$$\varepsilon_{Input\ CEC} = 4 \ln(D/E) \quad (2)$$

$$\varepsilon_{Exit\ Extrusion} = 2 \ln(D/X) \quad (3)$$

$$\varepsilon_{New\ CECAP} = \{1/\sqrt{3} [2 \cot(\varphi/2 + \psi/2) + \psi \csc(\varphi/2 + \psi/2)] + 4 \ln(D/E) + 2 \ln(D/X)\} \quad (4)$$

Where, E and X denote the input CEC and second extrusion diameters, respectively. Moreover, α_1 and α_2 represent the input CEC and exit extrusion angles with values of 60° , respectively. φ and ψ denote the channel angle and corner angle of the New CECAP die as illustrated in Fig. 1. The main vertical and horizontal channels diameters are denoted by D . As can be seen from Eq. (4), this relation is independent of the strain rate and frictional coefficient. Thus, their influences will be considered separately. The process was performed under isothermal conditions at a temperature of 300°C .

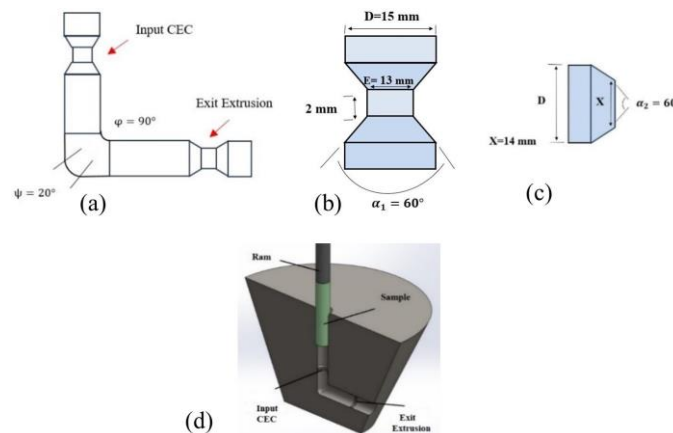


Fig. 1. (a) New CECAP, (b) input CEC, (c) exit extrusion, and (d) 3D model of the New CECAP process.

3. Experimental Procedure

Commercially pure titanium (CP-Ti) in the form of a cold-extruded rod was used in this study. Samples with a diameter of 15 mm and a length of 70 mm were machined from the as-received CP-Ti rod. The chemical composition of CP-Ti is presented in Table 1. To remove prior strain history and enhance plastic deformability, the samples were annealed at 750 °C for 120 minutes in a vacuum furnace, followed by furnace cooling to room temperature. All deformation processes were carried out at 300 °C with MoS₂ lubrication. Vickers microhardness measurements were conducted using a 30 g load, a 10-second dwell time, and a loading rate of 4 g/s. At each location, five indentations were made, and averaged to improve accuracy. The New CECAP die consisted of two symmetric halves with interchangeable inserts, as illustrated in Fig. 2.

The hot compression test was performed to extract the stress-strain behavior of CP-Ti in the current simulation. The tests were carried out at temperatures of 270 °C, 300 °C and 330 °C [10], and at strain rates of 0.01, 0.1 and 1. Fig. 3 illustrates the hot compression test sample. Finally, the stress-strain behavior obtained from the hot compression tests is presented in Fig. 4.

4. FEM Procedure

Commercial DEFORM-3D (Version 11) software was used to conduct the numerical simulations. The sample was modeled as a plastic cylindrical body with a diameter of 15 mm and a height of 70 mm. In the simulation, the CECAP die and ram were treated as rigid bodies. Friction

was modeled using the shear friction approach with a friction factor of $m = 0.5$, as recommended in [25]. Based on a mesh convergence study, a total of 55,000 tetrahedral elements were selected for meshing the sample to ensure simulation accuracy. All analyses were performed under isothermal conditions at 300 °C. The flow behavior of the material was described using the diagrams presented in Fig. 4. To accommodate the large plastic deformations involved in the process, an automatic remeshing system was employed throughout the simulation.

5. Results and Discussion

5.1. FEM results

A comparative analysis was performed among the ECAP, CECAP, and New CECAP processes in terms of effective strain, mean compressive stress, and damage distribution. To visualize the effective strain distribution, cross-sectional views were generated for the simulated samples for each process, as shown in Fig. 5. As observed in the figures, the effective strain obtained for the New CECAP process aligns well with the theoretical prediction provided by Eq. (4), with a maximum strain value of approximately 4. In this process, the total strain applied to the sample is distributed as follows: around 2 from the ECAP region, and approximately 1 each from both the input CEC and exit extrusion zones. In contrast, for the conventional CECAP process, due to the absence of the exit extrusion stage and lack of flow restrictions, the total effective strain is limited to about 3.

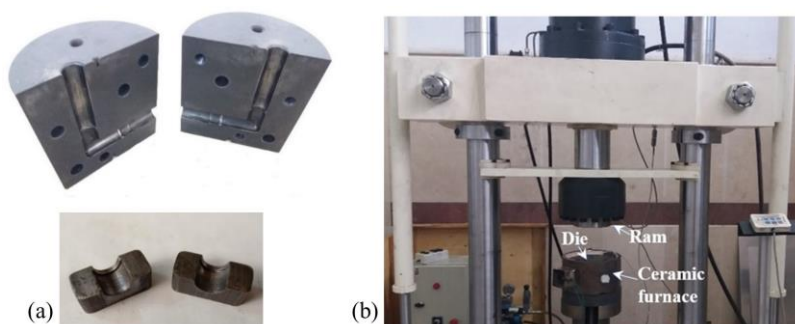


Fig. 2. (a) New CECAP die and inserts, (b) press used for experimental process.

Table 1. Chemical composition of the CP-Ti used in this study

Element	O	N	Fe	Pd	Mg	Cr	Ti
Volume percentage (%)	0.19	0.03	0.14	0.19	0.12	0.2	Balance

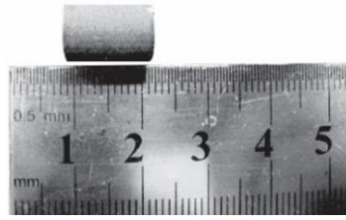


Fig. 3. Initial sample used for the compression test.

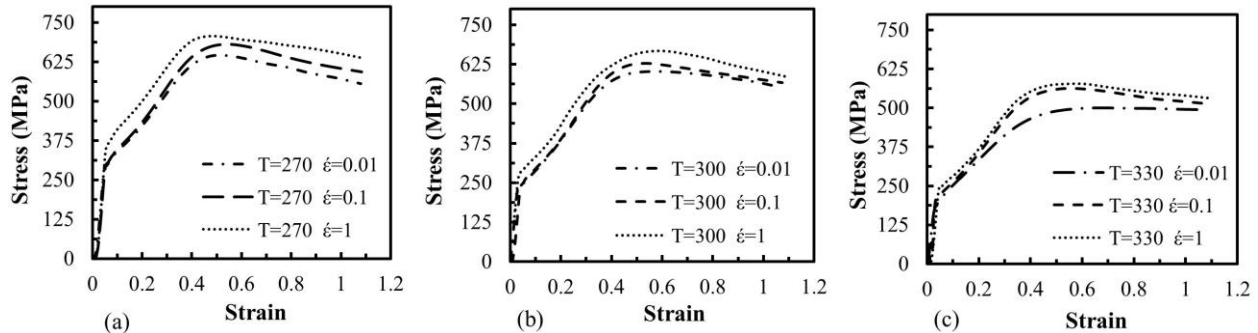


Fig. 4. Stress-strain behavior of CP-Ti obtained from the hot compression test at different temperatures and strain rates; (a) 270 °C, (b) 300 °C, and (c) 330 °C.

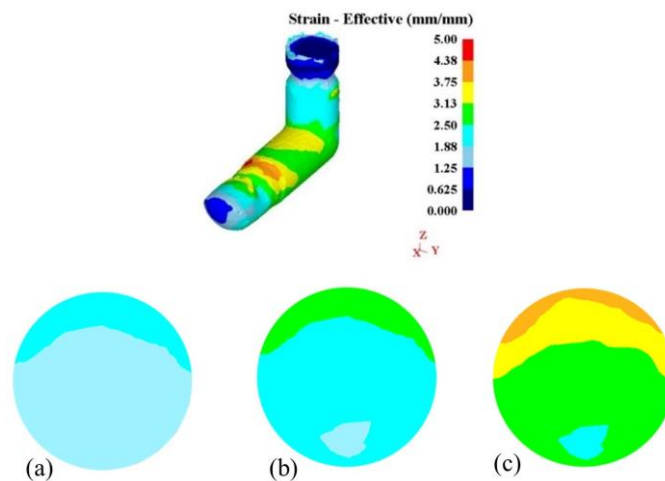


Fig. 5. Effective strain distribution for (a) ECAP, (b) CECAP, and (c) New CECAP.

The contour distribution of mean compressive (hydrostatic) stress for the three processes, ECAP, CECAP, and New CECAP is shown in Fig. 6 on a section perpendicular to the deformation axis, located before the ECAP region. Among the three, the New CECAP process exhibits the highest compressive stress, reaching a maximum value of approximately 190 MPa. This increase is attributed to the back pressure generated when the upper part of the sample enters the exit extrusion region. The diameter reduction in this region creates resistance to material flow, thereby elevating the compressive stress. Furthermore, a steeper extrusion angle increases this resistance, further contributing to stress buildup. The presence of the exit extrusion zone in

New CECAP also ensures complete filling of the ECAP region by the sample, which is one of the method's major advantages, as it helps prevent crack initiation. In contrast, the ECAP and CECAP processes, lacking this exit extrusion region, exhibit lower compressive stresses, with maximum values of -145 MPa and -180 MPa, respectively. The absence of back pressure in these methods increases the likelihood of crack formation during deformation. Moreover, in the New CECAP process, the mean compressive stress is distributed more uniformly across both the center and edges of the cross-section. This uniformity highlights the effectiveness of the method in promoting homogeneous stress distribution throughout the sample.

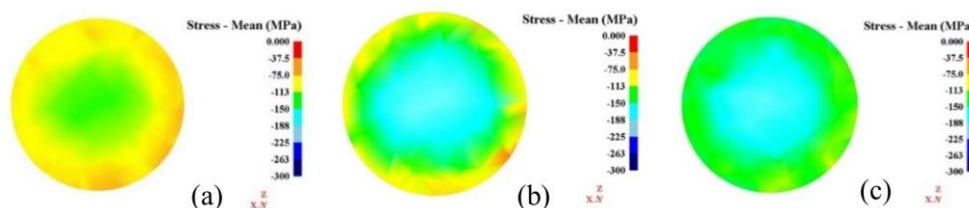


Fig. 6. Distribution of mean compressive stress (hydrostatic stress) for three processes: (a) ECAP, (b) CECAP, and (c) New CECAP.

Predicting the conditions that lead to sample failure is of critical importance in severe plastic deformation methods. To this end, various damage criteria have been developed to evaluate the workability of materials during plastic deformation. Among these, the Cockcroft–Latham criterion is widely used due to its simplicity and reliable predictive capability. The Cockcroft–Latham damage parameter is calculated using the following relation:

$$C = \int_0^{\varepsilon_f} \frac{\sigma_m}{\bar{\sigma}} d\bar{\varepsilon} \quad (5)$$

Where σ_m is the maximum tensile stress, $\bar{\varepsilon}$ is the equivalent plastic strain, and $\bar{\sigma}$ is the equivalent stress. According to this criterion, the cracks are expected to initiate when the damage factor reaches a critical value. Fig. 7 shows the variation of the Cockcroft–Latham damage factor across the cross-section of the deformed sample perpendicular to the movement axis (z-direction) for the three processes. The results indicate that, under all conditions, the probability of crack initiation increases from the lower surface toward the upper surface. Moreover, although the New CECAP process involves an additional deformation stage compared to CECAP resulting in greater plastic strain, the damage factor decreases and becomes more uniformly distributed. This behavior is attributed to the exit extrusion zone and the application of back pressure, which promote a more uniform and reduced damage distribution across the section.

The New CECAP process consists of three deformation operations, and can functionally be divided into six distinct stages, as listed in Table 2. To illustrate the variation of load during the process, the load–stroke diagram was developed, as shown in Fig. 8. The

diagram is divided into six segments corresponding to these stages. Part A represents the initial stage of the process, which includes the input CEC operation. During this stage, the load increases steadily, reaching up to 34 kN. Here, the input CEC region applies a diameter reduction of 2 mm to the sample, initiating the first plastic strain on the cylindrical sample with an initial diameter of 15 mm. In part B, the deformed sample moves through the space between the input CEC and ECAP regions without encountering resistance against the punch. Next, in part C, due to the resistance exerted at the end of the vertical cylindrical ECAP channel, the sample begins to expand, restoring its original diameter of 15 mm. At the end of this stage, the load rises to approximately 75 kN, and the sample undergoes ~11 mm of longitudinal deformation. During part D, the sample passes through the ECAP region, experiencing additional plastic strain; the load reaches around 120 kN. Part E corresponds to the passage of the sample through the region between the ECAP and exit extrusion zones, where no resistance to the punch is observed. Finally, in part F, the sample enters the exit extrusion region at the end of the horizontal channel. This zone applies a 1 mm diameter reduction and generates additional back pressure. The load–stroke curve for part F consists of two segments: an inclined section representing the exit extrusion deformation and a horizontal section corresponding to the subsequent movement of the sample without resistance.

Table 2. Different stages of the New CECAP process

A	Input CEC	D	ECAP region
B	Space between CEC and ECAP	E	Space between ECAP and exit extrusion
C	Diameter rise between CEC and ECAP	F	Exit extrusion

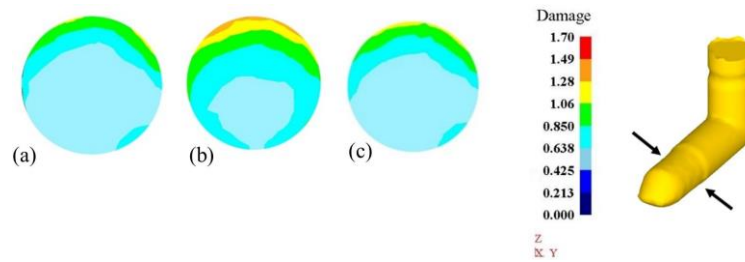


Fig. 7. Distribution of damage for three processes: (a) ECAP, (b) CECAP, and (c) New CECAP.

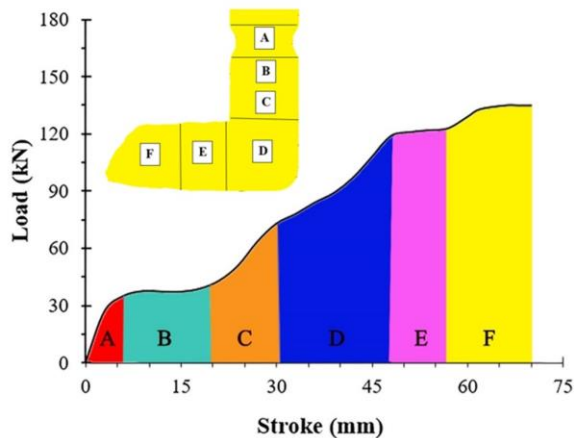


Fig. 8. Load for the different stages of the New CECAP process.

Fig. 9 illustrates the variations of damage and mean compressive stress during the New CECAP process at two points (A and B) along the longitudinal section of the sample. The mean compressive stress variations shown in Fig. 9(a) indicate that, at both points, stress decrease steadily during the first stage, reaching approximately -190 MPa. As the sample moves between the input CEC and ECAP regions, the mean compressive stress decreases further and approaches positive values. However, upon reaching the intersection of the two ECAP channels, the mean compressive stress at point B begins to decline again, as this location is on the inner side and experiences higher stress concentration. After passing through the ECAP region, the stress values at both points stabilize and show minimal variation. Finally, at around $t = 240$ s, due to the stress induced by the exit extrusion, the mean compressive stress at both points rises sharply, reaching approximately -345 MPa. Fig. 9(b) shows the variation of the damage factor with time. Both points follow a

similar increasing trend until $t = 175$ s, indicating continuous damage accumulation. Beyond this point, the damage factor at point B rises sharply, whereas the increase at point A is more gradual. In summary, along the longitudinal section of the sample, mean compressive stress and damage exhibit opposite trends: after the ECAP region, mean compressive stress becomes more negative, while damage continues to increase until the end of the process.

5.2. Experimental results and comparison with the numerical method

Fig. 10 shows the experimental samples of CP-Ti processed by the three different methods: New CECAP, CECAP, and ECAP. The experimental tests were conducted to measure hardness and cold compressive strength, and to validate the proposed numerical model. To this end, the effective strain distribution obtained from the simulations was compared with the hardness distribution measured on the experimental samples. Measurements were performed on the longitudinal section parallel to the movement axis of the fabricated samples, as illustrated in Fig. 10(d).

Fig. 11 shows the hardness values measured at different points across the cross-sections of samples processed by New CECAP, CECAP, ECAP, as well as the initial annealed and unannealed samples. Hardness tests were conducted in two directions, left to right and top to bottom, measuring five points along each path. The average and maximum hardness values were then calculated for each direction.

The results indicate that the average hardness of the annealed sample is 14 HRC, whereas samples processed

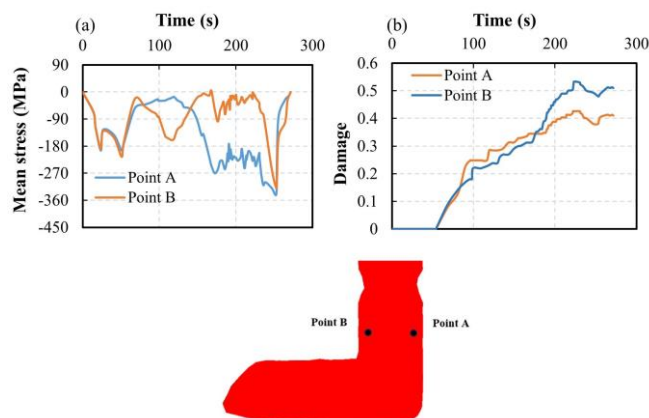


Fig. 9. Variations of (a) mean compressive stress, and (b) damage factor for two elements along the longitudinal section of the sample.

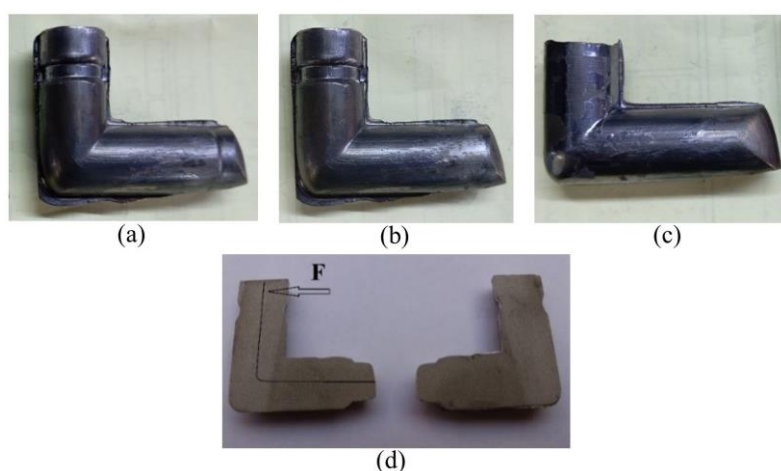
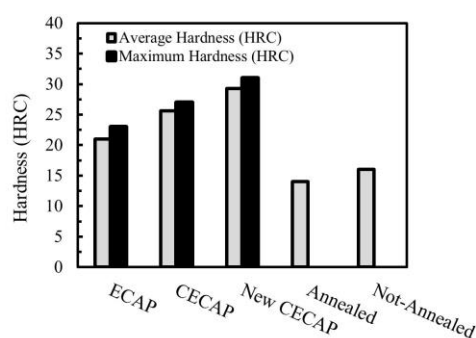


Fig. 10. Experimentally fabricated CP-Ti sample: (a) New CECAP, (b) CECAP, (c) ECAP, and (d) longitudinal section for hardness measurement.



Average hardness (HRC)	21	26	29.5	14	16
Maximum hardness (HRC)	23	27	31		

Fig. 11. Hardness distribution for unprocessed (annealed and not-annealed) and three different processes.

by ECAP, CECAP, and New CECAP exhibit hardness values of 21 HRC, 26 HRC, and 29 HRC, respectively. These results demonstrate the superior effectiveness of the New CECAP process in enhancing sample hardness. Based on the Hall-Petch relationship [23], this improvement can be attributed to the finer grain size in

the microstructure [24] produced by the New CECAP process. Additionally, the presence of mean compressive (hydrostatic) stress in the New CECAP process plays a significant role in increasing and homogenizing mechanical properties compared to ECAP and CECAP. Fig. 12 presents the distribution of hardness and effective

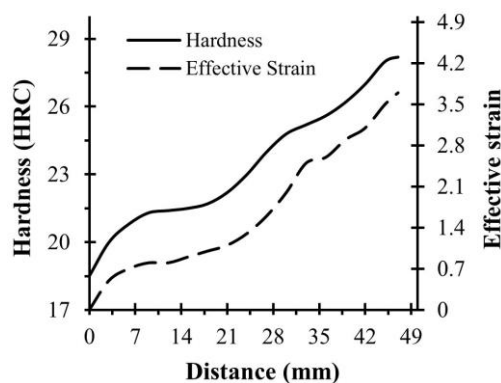


Fig. 12. Hardness distribution along the longitudinal section (path F) parallel to movement axis of the fabricated new CECAP sample.

strain along the sample's movement direction. The three increases observed along path F (shown in Fig. 10(d)) correspond to the input extrusion, ECAP, and exit extrusion regions. As observed, the trends in both hardness and strain closely match, confirming good agreement between numerical predictions and experimental results.

Fig. 13 presents the results of the cold compression tests conducted on samples processed by ECAP, CECAP, and New CECAP. The relative change in sample length during compression until failure was used as a measure of ductility. Interestingly, despite the inherently limited deformability of CP-Ti due to its HCP crystal structure, the highest ductility was observed in the ECAP-processed specimen. This can be attributed to the relatively lower plastic deformation during ECAP, which allows greater dislocation mobility compared to CECAP and New CECAP. For HCP-structured titanium, which lacks sufficient slip systems, mechanical properties are strongly influenced by grain size [23]. Additionally, microstructural evolution during hot forming is heavily affected by both the rate and magnitude of applied strain [25], with dynamic recrystallization (DRX) being the primary mechanism driving microstructural changes under intense plastic deformation in CP-Ti. Fig. 13 also shows elongation, yield strength, and ultimate tensile strength for the processed samples. Among the three processes, New CECAP exhibits the highest yield and ultimate strengths due to three consecutive deformation operations (input CEC + ECAP + exit extrusion), resulting in higher total plastic strain and more extensive activation of slip systems. Moreover, for CP-Ti, yield strength is influenced not only by grain size-dependent but also by texture evolution during severe plastic deformation (SPD) [23]. The New CECAP process produces a finer average grain size and promotes crystallographic texture development, particularly the formation of a basal texture, which significantly enhances mechanical properties like ultimate strength. In addition to grain refinement, New CECAP modifies texture and reduces microstructural defects, improving both strength and ductility. The development of new texture complements grain refinement by enhancing

plastic deformation capacity. Quantitatively, the ultimate strength increase from CECAP to ECAP samples is about 2%, indicating the effect of input CEC strain, whereas the increase from ECAP to New CECAP is more pronounced at 18%. With increased plastic deformation, the position of ultimate strength shifts leftwards on the stress-strain curve, with New CECAP samples showing the greatest shift, consistent with higher deformation. Despite the higher ultimate strength, New CECAP also improves elongation compared to ECAP and CECAP. This improved ductility is attributed to the exit extrusion step, which imposes additional strain, increases slip activity, creates back pressure, and promotes a more uniform strain distribution, reducing microstructural defects.

Fig. 13 further compares samples from as-received, ECAP, CECAP, and New CECAP conditions. Although CP-Ti naturally has limited ductility due to its HCP structure, the ECAP-processed sample shows the highest ductility among processed samples, despite a smaller uniform deformation region compared to as-received material. In terms of strength, New CECAP samples display the highest final strength due to the cumulative effect of the three deformation operations. The greater total strain leads to increased work hardening and grain refinement. Higher applied loads activate dislocations on multiple slip systems, including those with low Schmid factors, resulting in complex interactions and increased resistance to deformation. Additionally, New CECAP may induce a preferred grain orientation (texture) that lowers the Schmid factor in many grains, contributing further to increased strength.

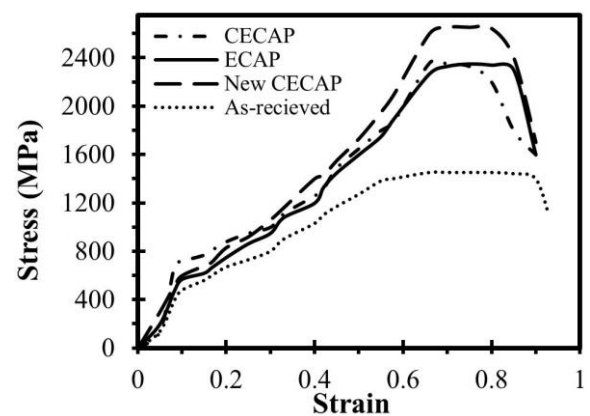


Fig. 13. Results of the cold compression test for as-received and three different processes.

The enhanced ductility in New CECAP samples, despite higher strains, is likely related to the formation of specific texture components, such as basal plane {0001} orientations, during the exit extrusion step. These texture changes reduce the material's resistance to deformation and prevent the development of deformation-resistant textures that would otherwise embrittle the material. In summary, the ultimate strength increase from CECAP to ECAP is about 2%, whereas from ECAP to New CECAP it reaches 18%. The New CECAP process also significantly improves ductility compared to CECAP, due to texture modification, more uniform strain distribution, and microstructural defect reduction enabled by the exit extrusion step.

Fig. 14 illustrates the load variations during the New CECAP, CECAP, and ECAP processes. As expected, the New CECAP process shows three distinct load increases corresponding to its three deformation stages. The first rise occurs during the input CEC stage, reaching about 7 tons. The load then sharply increases as the sample enters the ECAP zone, peaking around 20 tons. Finally, a third load increase is observed during the exit extrusion, reaching approximately 24 tons. These increments clearly reflect the sequential deformation steps in New CECAP. In contrast, the ECAP process shows a single

load rise, corresponding to the ECAP region, with a peak load of about 12 tons, followed by a steady load as the process continues. The CECAP process exhibits a load pattern similar to New CECAP but lacks the final increase associated with exit extrusion, as this step is absent. Fig. 14(a) compares the load-distance diagrams obtained from both experimental and numerical methods for all three processes. The trends are consistent: New CECAP exhibits three load increments, ECAP shows one, and CECAP shows two, without the exit extrusion peak. The close agreement between experimental and numerical results validates the accuracy of the numerical model. However, some discrepancies exist, such as a maximum load difference of about 25,000 N at the end of the New CECAP process, which is reasonable given model assumptions and material impurities. Overall, due to the two additional deformation steps (input CEC and exit extrusion), New CECAP requires a higher load throughout the process compared to ECAP and CECAP.

6. Conclusions

This research conducted a comparative investigation of ECAP, CECAP, and New CECAP processes through numerical simulations, validated by experimental results. The key findings are as follows:

- The New CECAP process was functionally divided into six stages, and the load-stroke diagram was examined. Part A represents the input stage, including the input CEC, with the load rising to 34 kN. In Part B, the deformed sample passes through the gap between the input CEC, and the ECAP region. In Part C, due to the resistance at the end of the vertical cylindrical ECAP channel the sample begins to expand, restoring its original shape (15 mm in diameter). In part D, the specimen passes through the ECAP region, receiving additional strains, where the graph shows 120 kN and continues to 17 mm. In part E, the sample moves through the distance between the ECAP and exit extrusion zone (~9 mm) without resistance. Finally, in part F, the sample enters the exit extrusion region at the end of the horizontal channel.

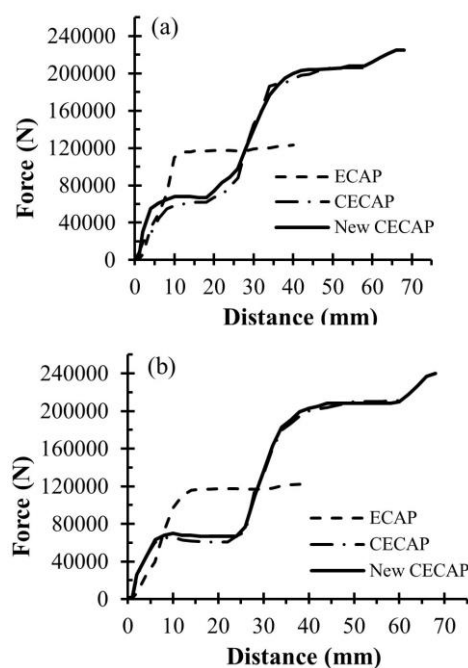


Fig. 14. Load-distance variations for (a) simulation, and (b) experimental results.

- The mean compressive stress reaches a maximum of ~ -190 MPa in the New CECAP process. This is due to the back pressure generated exit extrusion region, where the diameter reduction increases the compressive stress.
- Hardness measurements across different points in the sample sections for New CECAP, CECAP, ECAP, and annealed and non-annealed samples showed that the average hardness was 14 HRC for the annealed sample, and 21 HRC, 26 HRC, and 29 HRC for ECAP, CECAP, and New CECAP, respectively.
- The results of the cold compression test for samples obtained from ECAP, CECAP and the New CECAP show that the highest strength and performance were achieved by New CECAP. The ultimate strength from CECAP to ECAP samples increased by approximately 2%, indicating the effect of the input CEC strain on the sample, while the increase for New CECAP was about 18% compared to the ECAP process.

Authors' contributions

B. Pasoodeh: Data curation, Formal analysis, Investigation, Methodology, Validation, Writing – original draft

V. Alimirzaloo: Formal analysis, Investigation, Supervision, Validation, Writing – review & editing

M. Shahbaz: Data analysis, Methodology, Supervision, Writing – review & editing

K. Hajizadeh: Data analysis, Investigation, Writing – review & editing

J. Alizadeh Kaklar: Investigation, Writing – review & editing

Conflict of interest

All authors state that there are no potential conflicts of interest related to the submission of this article.

Funding

The authors declare that no funds, grants, or other support were received.

7. References

- [1] Levitas, V. I., (2019). High-pressure phase transformations under severe plastic deformation by torsion in rotational anvils. *Materials. Transaction*, 60, 1294-1301. <https://doi.org/10.2320/matertrans.MF201923>
- [2] Ivanisenko, Y., Kulagin, R., Fedorov, V., Mazilkin, A. Scherer, T., Baretzky, B., & Hahn, H., (2016). High pressure torsion extrusion as a new severe plastic deformation process. *Materials Science and Engineering: A*, 664, 247–256. <https://doi.org/10.1016/j.msea.2016.04.008>
- [3] Valiev, R. Z., Islamgaliev, R. K., Alexandrov, I. V., (2000). Bulk nanostructured materials from severe plastic deformation. *Progress in Materials Science*, 45, 103-189. [https://doi.org/10.1016/S0079-6425\(99\)00007-9](https://doi.org/10.1016/S0079-6425(99)00007-9)
- [4] Jiang, W., Cui, H., Song, Y., (2018). Electrochemical corrosion behaviors of titanium covered by various TiO₂ nanotube films in artificial saliva. *Journal of Materials Science*, 53(6), 15130-15141. <https://doi.org/10.1007/s10853-018-2706-5>
- [5] M. Kaur, K. Singh, (2019). Review on titanium and titanium-based alloys as biomaterials for orthopedic applications. *Materials Science and Engineering C*, 102, 844-862. <https://doi.org/10.1016/j.msec.2019.04.064>
- [6] Chehrehsaz, Y., Hajizadeh, K., Hajizadeh, A., Moradi, L., Mahshid, S. (2021). Effect of ECAP on physicochemical and biological properties of TiO₂ nanotubes anodized on commercially pure titanium. *Metals and Materials International*, 28, 1525-1535. <https://doi.org/10.1007/s12540-021-01003-9>
- [7] Indira, K. A., Mudali, U. K., Nishimura, T., & Rajendran, N. (2015). A review on TiO₂ nanotubes: influence of anodization parameters, formation mechanism, properties, corrosion behavior, and biomedical applications. *Journal of bio-and tribo-corrosion*, 1(4), 28. <https://doi.org/10.1007/s40735-015-0024-x>
- [8] Ensafi, M., Faraji, G., & Abdolvand, H. (2017). Cyclic extrusion compression angular pressing (CECAP) as a novel severe plastic deformation method for producing bulk ultrafine grained metals. *Materials Letters*, 197, 12-16. <https://doi.org/10.1016/j.matlet.2017.03.142>
- [9] Ahmadi, S., Alimirzaloo, V., Faraji, G., & Donyavi, A. (2020). A new modified cyclic extrusion channel angular pressing (CECAP) process for producing ultrafine-grained mg alloy. *Transactions of the Indian Institute of Metals*, 73(10), 2447-2456. <https://doi.org/10.1007/s12666-020-02048-x>
- [10] Hajizadeh, K., Eghbali, B., Topolski, K., & Kurzydowski, K. J. (2014). Ultra-fine grained bulk CP-Ti processed by multi-pass ECAP at warm deformation

- region. *Materials Chemistry and Physics*, 143(3), 1032-1038.
<https://doi.org/10.1016/j.matchemphys.2013.11.001>
- [11] Valiev, R. Z., & Langdon, T. G. (2006). Principles of equal-channel angular pressing as a processing tool for grain refinement. *Progress in materials science*, 51(7), 881-981. <https://doi.org/10.1016/j.pmatsci.2006.02.003>
- [12] Valiev, R. Z., Kozlov, E. V., Ivanov, Y. F., Lian, J., Nazarov, A. A., & Baudelet, B. (1994). Deformation behaviour of ultra-fine-grained copper. *Acta metallurgica et materialia*, 42(7), 2467-2475. [https://doi.org/10.1016/0956-7151\(94\)90326-3](https://doi.org/10.1016/0956-7151(94)90326-3)
- [13] Kawaski, M., & Langdon, T. G. (2018). Superplasticity in ultrafine-grained materials. *Reviews on advanced materials science*, 54, 46-55. <https://doi.org/10.1515/rams-2018-0019>
- [14] Zhang, J., Zhang, K. S., & Hwai-Chung, W. (2009). Experimental and numerical investigation on pure aluminum by ECAP. *Transactions of nonferrous metals society of China*, 19(5), 1303-1311. [https://doi.org/10.1016/s1003-6326\(08\)60442-2](https://doi.org/10.1016/s1003-6326(08)60442-2)
- [15] Patil, B. V., Chakkingal, U., & Kumar, T. P. (2010). Influence of outer corner radius in equal channel angular pressing. *World Academy of Science, Engineering and Technology*, 62, 714-720. <https://doi.org/10.13140/2.1.1135.4247>
- [16] Richert, M. W. (2006). Features of cyclic extrusion compression: method, structure & materials properties. *Solid State Phenomena*, 114, 19-28. <https://doi.org/10.4028/www.scientific.net/ssp.114.19>
- [17] Pardis, N., Talebanpour, B., Ebrahimi, R., & Zomorodian, S. (2011). Cyclic expansion-extrusion (CEE): A modified counterpart of cyclic extrusion-compression (CEC). *Materials Science and Engineering: A*, 528(25-26), 7537-7540. <https://doi.org/10.1016/j.msea.2011.06.059>
- [18] Amani, S., Faraji, G., & Abrinia, K. (2017). Microstructure and hardness inhomogeneity of fine-grained AM60 magnesium alloy subjected to cyclic expansion extrusion (CEE). *Journal of Manufacturing Processes*, 28, 197-208. <https://doi.org/10.1016/j.jmapro.2017.06.007>
- [19] Ahmadi, S., Faraji, G., Alimirzaloo, V., & Donyavi, A. (2021). Microstructure and mechanical properties of AM60 magnesium alloy processed by a new severe plastic deformation technique. *Metals and Materials International*, 27(8), 2957-2967. <https://doi.org/10.1007/s12540-020-00889-1>
- [20] Ebrahimi, M., Zhang, L., Wang, Q., Zhou, H., & Li, W. (2023). Damping performance of SiC nanoparticles reinforced magnesium matrix composites processed by cyclic extrusion and compression. *Journal of Magnesium and Alloys*, 11(5), 1608-1617. <https://doi.org/10.1016/j.jma.2021.07.024>
- [21] Ebrahimi, M., Zhang, L., Wang, Q., Zhou, H., & Li, W. (2021). Damping characterization and its underlying mechanisms in CNTs/AZ91D composite processed by cyclic extrusion and compression. *Materials Science and Engineering: A*, 821, 141605. <https://doi.org/10.1016/j.msea.2021.141605>
- [22] Huang, H., Guo, M., Zhang, W., Zeng, J., Yang, K., Bai, H., (2021). Numerical investigation on the bearing capacity of RC columns strengthened by HPFL-BSP under combined loadings. *Journal of Building Engineering*, 39, 102266. <https://doi.org/10.1016/j.jobe.2021.102266>
- [23] Abdolvand, H., Faraji, G., Shahbazi Karami, J., (2017). Microstructure and mechanical properties of AZ91 tubes fabricated by Multi-pass Parallel Tubular Channel Angular Pressing. *Journal of Ultrafine Grained and Nanostructured Material*, 50, 16-22. <https://doi.org/10.7508/jufgns.2017.01.03>
- [24] Pande, C. S., & Cooper, K. P. (2009). Nanomechanics of Hall-Petch relationship in nanocrystalline materials. *Progress in Materials Science*, 54(6), 689-706. <https://doi.org/10.1016/j.pmatsci.2009.03.008>
- [25] Altan, T., (2004). *Cold and Hot Forging*. American Society for Metals, 50-53